**A tale of two catchments: Causality analysis and isotope systematics reveal mountainous watershed traits that regulate the retention and release of nitrogen**

Bouskill NJ[1][*], Newcomer M[1], Carroll RWH[2,3], Beutler C[3], Bill M[1], Brown WS[3], Conrad M[1], Dong WS[1], Falco N[1], Maavara T[4], Newman A[3], Sorensen PO[1], Tokunaga TK[1], Wan J[1], Wainwright H[1], Zhu Q[1], Brodie EL[1], Williams KH[1,3]

[1]Earth and Environmental Sciences Area, Lawrence Berkeley National Laboratory, Berkeley, CA, USA.
[2]Desert Research Institute, Reno, NV, USA.
[3]Rocky Mountain Biological Laboratory, Gothic, CO, USA.
[4]School of Geography, University of Leeds, UK.

*Corresponding author: njbouskill@lbl.gov

**Abstract**

Mountainous watersheds are characterized by variability in functional traits, including vegetation, topography, geology, and geomorphology, which together determine nitrogen (N) retention, and release. Coal Creek and East River are two contrasting catchments within the Upper Colorado River Basin that differ markedly in total nitrate ($NO_3^-$) export. The East River has a diverse vegetation cover, sinuous floodplains, and is underlain by N-rich marine shale, resulting in a three to twelve times greater total $NO_3^-$ export relative to the conifer-dominated Coal Creek. While this can partly be explained by the larger size of the East River, the distinct watershed traits of these two catchments imply different mechanisms controlling the aggregate N-export signal. A causality analysis shows biogenic and geogenic processes were critical in determining $NO_3^-$ export from the East River catchment. Stable isotope ratios of $NO_3^-$ ($\delta^{15}N_{NO3}$ and $\delta^{18}O_{NO3}$) show the East River catchment is a strong hotspot for biogeochemical processing of $NO_3^-$ at the soil-saprolite interface and within the floodplain prior to export. By contrast, the conifer-dominated Coal Creek retained nearly all (~97 %) atmospherically-deposited $NO_3^-$, and its export was controlled by catchment hydrological traits (i.e., snowmelt periods and water table depth). The conservative N-cycle within Coal Creek is likely due to the abundance of conifer trees, and a smaller riparian region, retaining more $NO_3^-$ overall and reduced processing prior to export. This study highlights the value of integrating isotope systematics to link watershed functional traits to mechanisms of watershed element retention and release.

**Plain Language Summary**

The role different functional traits play in the retention and release of nitrogen remains uncertain. Here we describe how two neighboring catchments in the Upper Colorado River Basin, characterized by contrasting vegetation, geology, and geomorphology, cycle and export nitrogen. The East River catchment, which is underlain by nitrogen-rich shale, and has a diverse vegetation cover, releases three to twelve-times as much nitrate ($NO_3^-$) than the conifer-dominated Coal Creek, which is underlain by granitic rock. However, a suite of analyzes show that the distinct watershed traits of these two-catchments lead to diverse emergent pathways of nitrogen cycling. Biogenic and geogenic processes, critical to determining $NO_3^-$ export in East River, impart strong biogeochemical processing prior to export. By contrast, Coal Creek retains almost all of the atmospherically-deposited $NO_3^-$, likely due to uptake by conifers, and a small riparian region. This study highlights the use of nitrate isotope systematics to parse different mechanisms leading to $NO_3^-$ export.

**Key points**

- Comparing and contrasting neighboring catchments permits the identification of watershed traits regulating the cycling, retention and release of nitrogen (N).
- Conifer forest-dominated catchments show a conservative nitrogen cycling, retaining ~97 % of atmospherically dominated nitrate.
- By contrast, meadow-dominated catchments underlain Mancos shale are biogeochemical hotspots for N-cycling, and export higher nitrate loads.

120

## 1. Introduction

122

123 Strong variability in stream water chemistry between neighboring headwater catchments can

124 provide insight into how watershed traits (e.g., gradients in bedrock, topography, aspect, and

125 land cover) interact to modulate retention and release of critical elements and thus influence

126 downstream water quality (Alexander et al., 2007; McDonnell et al., 2007). Nitrogen, which

127 often limits ecosystem processes within mountainous watersheds (Campbell et al., 2002; Kou et

128 al., 2020; Thébault et al., 2014), enters through several pathways, including by atmospheric

129 deposition of inorganic and organic nitrogen (Clark et al., 2021), bedrock weathering (Holloway

130 et al., 1998; Houlton et al., 2018; Wan et al., 2021), and nitrogen fixation (Moyes et al., 2016).

131 Retention within the ecosystem occurs primarily through plant acquisition, microbial

132 immobilization (Goodale, 2017; Zogg et al., 2000), and groundwater storage (Ascott et al.,

133 2017). Loss of nitrogen occurs through denitrification within variably saturated regions of the

134 watershed (e.g., within floodplains, Bouskill et al., 2019; Gomez-Velez et al., 2015), the

135 erosional deposition of particulate nitrogen (Berhe & Torn, 2017), or lateral flow of dissolved

136 species to streams and rivers (Peterson, 2001; Rose et al., 2015).

137

138 The balance between the retention and release of nitrogen in headwater catchments is strongly

139 coupled to the hydrological cycle (Maavara et al., 2021; Wan et al., 2021; Schimel et al., 1997;

140 Zhu et al., 2018). The transit times of different solutes through the terrestrial biosphere are

141 dictated by the contact time between water and reactive surfaces including microorganisms

142 (Lansdown et al., 2015; Li et al., 2021; Pinay et al., 2015). The resultant stream water chemistry

143 is derived from distinct water sources that reflect this transit time, and the magnitude of

144 biogeochemical cycling of nitrogen along the various flow paths to the river. Depending on the

145 time of year within snowmelt-dominated systems, the chemical signatures might reflect nitrogen

146 derived from flow paths across distinct hillslope depths (Zhi et al., 2019; Zhi et al., 2020),

147 whereby shallow soils dominate solute flux to the river as the water table rises towards the

148 surface during snowmelt (Zhi et al., 2019). By contrast, stream water chemistry likely reflects the

149 deeper groundwater-dominated sources under baseflow conditions.

150

151      The movement of water and nitrogen through the subsurface of mountainous catchments is also

152      further modified through interactions with vegetation. Plant-nitrogen assimilation predominantly

153      takes place from shallow soil layers, aided by the turnover of microbial biomass built-up under

154      snowpack (Sorensen et al., 2020). Mycorrhizal-symbionts further regulate nutrient transfer from

155      soils to plants (Hobbie & Högberg, 2012), and the relationship between plants and different

156      mycorrhizal fungi shapes the nitrogen sources that can be accessed (Phillips et al., 2013; Ward et

157      al., 2022). Moreover, the flux of nitrogen entering catchments is also dependent on litter

158      decomposition is a function of litter quality (e.g., carbon: nitrogen ratios), which is a function of

159      species demographics and a critical pathway of the nitrogen cycle in high-altitude soils (Maavara

160      et al., 2021). Catchment heterogeneity results in the emergence of different plant communities,

161      which, subsequently plays an important role in determining aggregate nitrogen retention and

162      release (Newcomer et al., 2021).

163

164      This study details how nitrogen is cycled and exported as a function of headwater catchment

165      traits. We compare and contrast the nitrogen cycles of two catchments, Coal Creek and the main

166      stem East River, within the wider East River watershed in the Upper Colorado River Basin,

167      United States. Although separated by less than 7 kilometers, these snowmelt-dominated

168      catchments differ in their underlying traits, notably geology, dominant vegetation,

169      geomorphology, and aspect (Hubbard et al., 2018). In contrast, rates of atmospheric nitrogen

170      deposition to the two catchments are similar and extremely low (~2-3 kg ha$^{-1}$ yr$^{-1}$), meaning that

171      underlying catchment traits dominate the differences in nitrogen retention and release. Herein we

172      examine whether the contrasting biotic and abiotic traits that distinguish Coal Creek and the East

173      River are apparent through contrasting signals in nitrogen export.

174

175      To test this supposition, we analyze concentration-discharge (cQ) relationships of biogenic and

176      geogenically derived solutes across a five-year data time series from both Coal Creek and East

177      River catchments. cQ relationships have been widely used to determine how different

178      catchments store and release water and solutes (Knapp et al., 2020), and to partition between

179      geogenic and biogenic sources as a function of the hydrograph (Zhi et al., 2019). The cQ

180      relationship is often described by a power law between the logarithms of both variables ($c=aQ^b$),

181      where $a$ represents the intercept and the exponent, $b$, represents the slope of the cQ relationship

182    (Musolff et al., 2015). The exponent provides information determining how the relationship

183    between solute export changes with the hydrograph (Thompson et al., 2011). For example, $b = 0$

184    indicates a chemostatic relationship between discharge and solute concentration, a relationship

185    characteristic of headwater catchments (Godsey et al., 2009). By contrast, positive or negative

186    deviations from this relationship can represent solute mobilization (e.g., from shallow soil

187    reservoirs), or dilution (common for geogenically derived solutes), respectively (Knapp et al.,

188    2020; Musolff et al., 2015; Zhi et al., 2020). However, the power law characterization of the cQ

189    is insensitive to high variability in data, which can be the case for nutrients such as $NO_3^-$ and

190    attributable to heterogeneity in landscape properties and hydrologic connectivity that influence

191    groundwater table fluctuations, redox conditions, and elemental mobility (Thompson et al.,

192    2011). We therefore combine the power law analysis with an analysis of the ratio between the

193    coefficient of variation (CV) of concentration ($CV_c$) and discharge ($CV_c/CV_q$), which can further

194    contextualize whether the underlying relationship in solute export is driven by variability in

195    discharge, improving understanding of solute mobilization (Knapp et al., 2022). For example, a

196    $CV_c/CV_q$ ratio $\leq 0.5$ indicates that the variability in discharge ($CV_q$) is greater than the variability

197    in solute concentrations ($CV_c$), and is therefore, chemostatic. By contrast, a high solute

198    concentration variability, relative to discharge ($CV_c/CV_q \geq 0.5$), the relationship might be

199    considered chemodynamic.

200

201    Neither metric described above attributes solute export to an underlying mechanism, therefore

202    this analysis is combined with measurements of the stable isotopes of nitrate ($\delta^{15}N_{NO3}$ and

203    $\delta^{18}O_{NO3}$) from both soil porewater, as well as Coal Creek and East River. The isotopic signature

204    of nitrate represents the aggregated contribution of different sources and reflects both the

205    strength of retention and the magnitude of biogeochemical cycling along different flow paths

206    towards the river (Granger & Wankel, 2016). $\delta^{15}N_{NO3}$ and $\delta^{18}O_{NO3}$ can identify periods of high

207    nitrate reduction through the monotonic enrichment in isotopic fractionation (Wexler et al.,

208    2014), indicating prolonged transit times through the ecosystem. Moreover, the direct

209    contribution of atmospheric nitrate to riverine export can be identified through high $\delta^{18}O_{NO3}$ ($\sim$60

210    - 80 ‰) imparted during the atmospheric formation of nitrate (Michalski et al., 2012), and this

211    isotopic signal can be used to quantify retention of atmospheric nitrate by vegetation and

212    microbes.

213

214 We use these complementary data sets to address two main objectives: Our first objective seeks

215 to compare and contrast nitrate export within two neighboring catchments differing in functional

216 trait distribution while sharing the same climate and nitrogen deposition patterns. A second

217 objective focuses on the East River catchment and leverages existing borehole infrastructure, not

218 currently available in Coal Creek, to relate riverine nitrate export to nitrogen cycling across a

219 hillslope-toeslope-floodplain continuum adjoining the river.

220

221 **2. Materials and Methods**

222

223 *2.1. Study Site*: The East River watershed (38° 57.5' N, 106° 59.3' W) is a representative

224 headwater system in the West Elk Mountains near the towns of Crested Butte and Gothic,

225 Colorado (USA) within the Upper Colorado Basin (Hubbard et al., 2018). The East River is a

226 major tributary to the Gunnison River, which accounts for almost half of the Colorado River's

227 discharge at the border with Utah. The East River watershed is approximately 300 km$^2$ (Fig. 1),

228 and encompasses the main stem East River (including the current study site East River at

229 Pumphouse), Slate River, Washington Gulch, and Coal Creek (Fig. 1a). The East River

230 watershed is a large watershed of the hydrologic unit code 10 (USGS: HUC10 East River

231 Watershed: #1402000102)), characterized by the intersection of two HUC12 catchments. The

232 East River at Pumphouse is made up of the smaller HUC12 catchments (#140200010201 Upper

233 East River) which drains to the HUC12 #140200010202 Brush Creek catchment where the

234 Pumphouse is located. For clarity, the catchment, East River at Pumphouse, is hereafter referred

235 to as ERP, to avoid confusion with the larger East River watershed. Coal Creek is a defined

236 HUC12 catchment (#140200010204 Coal Creek) of the HUC10 East River Watershed

237 (#1402000102).

238

239 The East River watershed has an average elevation of 3266 m, and ranges from 2750 to 4000 m

240 (Fig. 1b). The area has a continental, subarctic climate, with a mean annual temperature of 0°C,

241 and average minimum and maximum temperatures of -9.2 and 9.8°C, respectively. Mean annual

242 precipitation is ~1200 mm yr$^{-1}$, with the majority (> 80 %) falling as snow, and much of the rest

243 falling during the monsoonal period in late summer and fall (Carroll et al., 2020). Snowfall and

244  melt dominate the hydrological cycle, as is typical for mountainous systems in the Western

245  United States (Li et al., 2017), and losses are partitioned between evapotranspiration and

246  streamflow, which differ in their contributions based on several characteristics, including a

247  higher ET flux with higher proportional tree cover (Sprenger et al., 2022). Runoff characteristics

248  for both catchments are similar in terms of the timing of peak discharge in early June and the

249  transition to baseflow in late September-early October, where groundwater represents a

250  significant fraction of streamflow (Hubbard et al., 2018).

251

252  Atmospheric deposition of wet and dry forms of reactive nitrogen (nitrate and ammonium) for

253  the East River watershed was extracted from the EPA CASTNET continuous monitoring system

254  located at Gothic (https://www3.epa.gov/castnet/site_pages/GTH161.html), and from the broader

255  national atmospheric deposition program (https://nadp.slh.wisc.edu/committees/tdep/). Annual

256  nitrogen deposition averaged 2 - 3 kg-N ha$^{-1}$ over a 17-year period (2000-2017), split equally

257  between reduced and oxidized inorganic nitrogen (Fig. S1).Over that period the magnitude of

258  total nitrogen deposited into the watershed remained relatively constant, but the contribution

259  from ammonia roughly doubled, while that from nitrate fell, consistent with other regions of the

260  Rocky Mountains (Clark et al., 2021), and likely attributable to a lack of regulation on $NH_4^+$

261  emissions (Li et al., 2016).

262

263  Figure 1: The East River watershed depicting (a) land cover and (b) elevation. On each panel the
264  different catchments are demarcated by a black outline. With the Coal Creek catchment the river
265  sampling point is denoted by the orange diamond, while the orange circle in the East Tiver
266  catchment indicates the river sampling point, and the adjacent borehole transect for terrestrial
267  porewater collection.
268
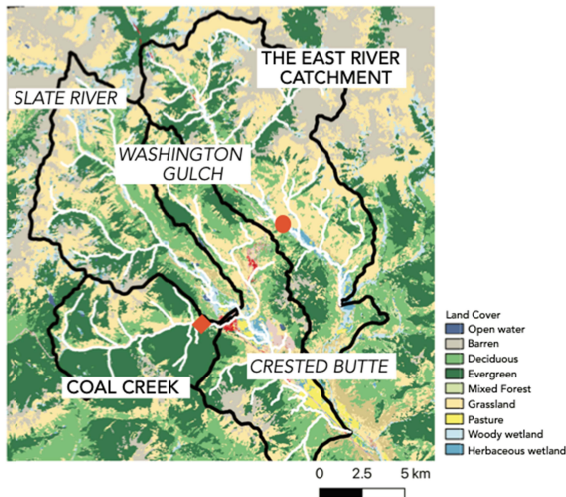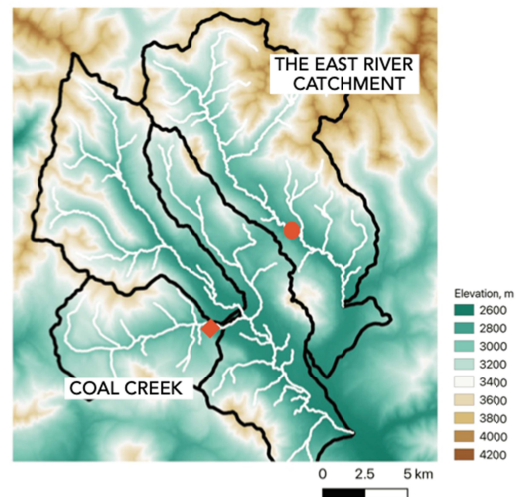
269

270

271    A recent analysis for the wider East River watershed separates these two catchments based on

272    their comparative disparity in traits including catchment size, aspect, average slope, vegetation

273    (including normal difference vegetation index), and geology (Wainwright et al., 2022). At 56

274    km$^2$, Coal Creek exhibits an east-west orientation, with north- and south-facing hillslope aspects,

275    and an average slope of 16$^\circ$. The characteristics of this catchment have been described

276    previously (Zhi et al., 2020). The land cover is approximately 60 % evergreen forests (e.g., *Picea*

277    *spp., Abies spp., Pinus contorta*) with 10 % montane plants and shrubs (e.g., *Artemisia*

278    *tridentata*), and 11 % riparian shrubland (dominated by *Salix monticola*). Only 1 % of land is

279    barren. The underlying bedrock is dominated by sedimentary and igneous rock types (including

280    areas of significant mineralization by pyritic ore minerals and associated historic mines). These

281    primarily include sandstone (39 %) and mudstone (15 %) from the Late Cretaceous Mesa Verde

282    formation and Neogene Ohio Creek and Wasatch formations (Manning et al., 2008; Uhlemann et

283    al., 2022). Supplementing these sedimentary units are plutonic rocks (15 %) dominated by

284    granodiorite and quartz monzonite of Oligocene age.

285

286    By contrast, the 86 km$^2$ main stem of the ERP intensive study site is oriented in a northwest-

287    southeast direction, with an average slope 23$^\circ$. Land cover within the ERP is more heterogeneous

288    than that of Coal Creek, with extensive regions of barren alpine and subalpine land, mixed forest,

289    including ~10 % deciduous forest (*Populus tremuloides*), ~21 % coverage by coniferous trees

290    (predominantly *Picea engelmannii, and Abies lasiocarpa*), and 27 % intermixed shrub- and

291  grassland meadows. The meadow regions show a mix of perennial bunchgrass (e.g., *Festuca*

292  *arizonica*), forbs (e.g., *Potentilla gracilis, Veratrum californicum, Lupinus spp.*), and shrubs

293  (*Artemisia tridentata*). Relative to Coal Creek, the East River shows considerable sinuosity, and

294  has an extensive riparian floodplain system dominated by dwarf birch (*Betula grandulosa*) and

295  mountain willow (*Salix spp.*). Plant communities are largely underlain by Cretaceous Mancos

296  shale bedrock (Hubbard et al., 2018), which is entirely absent in Coal Creek, with glacial till also

297  underlying the North Eastern end of the catchment. Agricultural influence is limited to summer

298  grazing of cattle within the ERP.

299

300  *2.2. Borehole installation:* To link export patterns to nitrogen cycling within terrestrial

301  ecosystems, we focused on a montane hillslope within the pumphouse intensive research site at

302  the East River. Five 10-m deep boreholes (0.14 m diameter) were drilled into bedrock along a

303  137 m-long hillslope-toeslope-floodplain transect. Specific drilling and instrumentation details of

304  these boreholes have been published previously (Wan et al., 2021), however, pertinent here was

305  the installation of porewater samplers, and moisture sensors from the O-horizon, through the

306  weathered saprolite, into the bedrock at >8 m across the transect. Porewater samples were taken

307  throughout the 2017-2019 period, inclusive of two anomalously high- and low-snowpack years.

308

309  *2.3. Physicochemical measurements:* We collected measurements of streamflow and stream

310  water chemistry across a 5-year, 9-month period covering January 1st, 2016 through September

311  30, 2021. The analysis of the streamflow data has been described recently (Carroll et al., 2021).

312  Stream- and porewater samples were collected for aqueous chemistry measurement using an

313  automatic sampler (Teledyne ISCO 3700, NE, USA) attached to a peristaltic pump. Sampling

314  frequency for stream water samples varied from once per week to three times per week

315  depending on season. Snow was sampled synoptically by digging snow pits and sampling down

316  through the depth of the pit. This depth was dependent on the snow year and varied between 0.4

317  and 1.6 m. Precipitation samples were also taken synoptically during the monsoonal period,

318  which typically spans the late June to early September timeframe. Prior to anion or cation

319  analysis, water samples were filtered through a 0.45 μm Millipore filter. The anion samples were

320  collected into 2ml polypropylene vials (with no headspace), and the cation samples were

321  collected into high-density polyethylene vials, and acidified with ultra-pure concentrated nitric

322    acid. Anions were measured through ion chromatography (Dionex ICS-2100, Thermo Scientific,

323    USA), and aqueous cation concentration was determined using ICP-MS (Elan DRC II, Perkin

324    Elmer, USA). Dissolved total nitrogen (DTN) was measured on all samples via thermal

325    decomposition and chemiluminescence (Shimadzu TOC-VCSH with the attached TNM-1).

326    Water samples for the determination of ammonium concentrations were taken as described above

327    and measured on a Lachat (QuikChem 8500 series 2 flow injection analysis system).

328

329    *2.4. Nitrate isotope measurements*: The natural abundance of $\delta^{15}N_{NO3}$ and $\delta^{18}O_{NO3}$ in riverine and

330    porewater, snow, and rainfall were measured using the denitrifier method as described previously

331    (Bouskill et al., 2019), and in detail in the supplemental materials. Briefly, samples from either

332    the river (40 ml) or lysimeters (50 - 100 ml) were filtered through a 0.2 μm Sterivex filter and

333    placed on ice in the field. Samples were shipped overnight to Lawrence Berkeley National

334    Laboratory and kept at -80°C until analysis. The isotope ratios of $NO_3^-$ ($\delta^{15}N_{NO3}$ and $\delta^{18}O_{NO3}$),

335    where $\delta$ (‰) = ($R_{NO3}$/ $R_{std}$ -1)*1000, R indicates either $^{15}N/^{14}N$ or $^{18}O/^{16}O$, and 'std' refers to

336    standard reference material, either $N_2$ in the air for $\delta^{15}N$ or Vienna standard mean ocean water

337    (VSMOW) for $\delta^{18}O$, were measured via the denitrifier method (Casciotti et al., 2002; Sigman et

338    al., 2001). Analysis of the isotopic data is described in detail in supplemental materials. Briefly,

339    we used a simple mixing model to partition the isotopic signal of riverine $NO_3^-$ between

340    atmospheric and soil-derived sources. Furthermore, the change in $\delta^{15}N_{NO3}$ relative to that of

341    $\delta^{18}O_{NO3}$ (i.e., $\Delta\delta^{18}O_{NO3}$: $\Delta\delta^{15}N_{NO3}$) was used in stream and poreater to determine whether a

342    decline in $NO_3^-$ concentrations could be due to source water mixing or due to fractionation

343    mechanisms, as described previously (Granger and Wankel, 2016).

344

345    *2.5. Analysis of concentration-discharge relationships:* Streamwater cQ relationships were

346    initially described using a power law relationship ($c=aQ^b$) for the whole data-set (which was log-

347    transformed prior to analysis), and broken down for each water year (2016-2021). We further

348    calculated the coefficient of variation of solute concentration ($CV_c$) and discharge ($CV_q$) (Basu et

349    al., 2011; Knapp et al., 2022; Thompson et al., 2011), using a previously published approach for

350    log-normal data (Knapp et al., 2022),

351

$$CV = \frac{\sigma}{\mu} = \frac{exp(m_{ln} + 0.5s_{ln}^2)}{exp(2m_{ln} + s_{ln}^2)(exp(s_{ln}^2) - 1)} = \sqrt{exp(s_{ln}^2) - 1} \qquad 1$$

352

353

354    where $m_{ln}$ and $s_{ln}$ represent the mean and standard deviation of the data.

355

356    *2.6. Causality analysis with information theory:* To contextualize watershed nitrate export

357    alongside the factors determining transit and loss through the watershed we treat the time series

358    of different hydrological, physical, biogenic, and geogenic data (from 2016 - 2021) as a coupled

359    process network (Ruddell & Kumar, 2009). Herein, the directional impacts from one process

360    (e.g., geogenic leaching, or snowmelt) to the other (e.g., nitrate export) is be quantitatively

361    inferred by Shannon information entropy (*H*) and its transfer (TE) (unit bits).

362

$$H = -\sum_{i=1}^{n} p(X_i)log_2 p(X_i) \qquad 2$$

363

$$T_{X->Y} = \sum_{y_i, y_{i-1}, x_{i-j}} p(y_i, y_{i-1}, x_{i-j}) log_2 \frac{p(y_i|y_{i-1}, x_{i-j})}{p(y_i|y_{i-1})} \qquad 3$$

364

365    where *p(x)* is probability density function (PDF) of *x*, *p(y$_i$,y$_{i-1}$,x$_{i-j}$)* is the joint PDF of current time

366    step *y$_i$*, previous time step of *y$_i$*, and *j*th time step before of *x$_i$*. *p(y$_i$|y$_{i-1}$,x$_{i-j}$)* and *p(y$_i$|y$_{i-1}$)* denote

367    conditional PDF of the corresponding variables. For example, the information entropy transfer

368    from snowmelt to nitrate export is calculated as Shannon entropy reduction (uncertainty

369    reduction) of present nitrate export given the historical snowmelt records (up to12 month time

370    lags) and excluded the influence from the previous time step for nitrate export. In order to ensure

371    the calculated transfer entropy does not stem from randomness, we conduct statistical

372    significance tests by first randomly shuffling the time series 10 times to obtain a distribution of

373    transfer entropy assuming the random shuffle will break the causality between SWE and

374    $NO_3^{EXPORT}$. Then a significance threshold of $TE^{SWE} -> NO_3^{EXPORT}$ is determined by the 95%

375    confidence threshold of the shuffled transfer entropy (Yuan et al., 2022). We report causality

376    only when the $TE^{SWE} \text{–>} NO_3^{EXPORT}$ of the original time series data is larger than its significance

377    threshold. We applied this causality modeling approach to the observed time series of watershed

378    variables at both the Coal Creek and ERP. The factors included in the analysis were chosen as

379    proxies for the different sources contributing stream $NO_3^-$, and included biogenic solutes derived

380    from shallower soils (e.g., DOC), or deeper bedrock derived solutes (e.g., Mg), redox active

381    compounds (e.g., $SO_4^{2-}$), and hydrological variables influencing nutrient flux and riverine

382    turnover (e.g., SWE and water temperature). Their relevance to $NO_3^-$ was visualized in a network

383    (Bastian et al., 2009) from which quantitative associations between different variables can be

384    identified.

385

386    *2.7. Assessment of annual and snowmelt nitrate export:* We calculated a time-series of total mass

387    exports leaving the Coal Creek and ERP catchments *Ex(t)* (Mg/year) using the discharge *Qs(t)*

388    and concentration *Cn(t)* time series by integrating from day 1 of each water year to day 365 for

389    annual time series, and during the specific time periods related to snowmelt (Equation 4). The

390    mass export is the multiplication of discharge *Qs(t)* (m$^3$/s) and concentration of nitrate *Cn(t)*

391    (mg-N/L converted to kg/m$^3$) and summed for all daily time steps (dt):

392

$$Export = Ex(t) = \sum_{day\ 1}^{day\ 365} Qs(t)Cn(t)dt \qquad 4$$

393

394    Discharge and concentration time series were gap-filled and interpolated using an averaging

395    method when missing values exist. N exports (Mg/year) were converted to N yields by dividing

396    by the area of each catchment and converting mass from Mg to kg to match the units of

397    atmospheric deposition (kg/hectare/year). We relate solute fluxes from inputs (e.g., atmospheric

398    deposition) to the riverine outputs through equation 5 which describes the retention of N within

399    each watershed on a water year basis:

400

$$Retention\ Capacity = Ret\% = \frac{Deposition - Yields}{Deposition} * 100 \qquad 5$$

401

402    In addition to input from atmospheric sources we also evaluate the potential contributions to

403    $NO_3^-$ export from bedrock weathering within the ERP. Correcting the estimated annual $NO_3^-$ flux

404    from the Mancos Shale saprolite of (Wan et al., 2021) with improved flow rates (Tokunaga et al.,

405    2022) results in 2.0 kg ha$^{-1}$ yr$^{-1}$ from the critical zone of a hillslope to the floodplain. Only a

406    fraction of this hillslope value is likely to reach the river due to denitrification while traversing

407    the floodplain. Furthermore, this value is unlikely to be representative of the watershed scale

408    hillslope weathering flux as parts of the watershed is underlain by glacial till, not shale, while

409    infiltration within north facing slopes (where these initial measurements were made) is higher

410    than south-facing slopes, promoting higher rates of weathering. For these reasons, we assume a

411    smaller range (0-1 kg ha$^{-1}$ yr$^{-1}$) of $NO_3^-$ derived from shale weathering likely contributes to the

412    catchment $NO_3^-$ export.

413

414    **3. Results**

415

416    *3.1. Concentration-discharge relationships:* The time span of this study covered both historical

417    highs and lows of snow water equivalence (SWE, m) and discharge (Q, m s$^{-1}$) within Coal Creek

418    and ERP. Both 2017 and 2019 were above average snowpack depth and discharge, while 2018

419    represented a historic low. Figure 2 provides the time course of SWE for the East River

420    Watershed, and Q for the specific regions. While the temporal trends in snowmelt driven

421    discharge were the same between Coal Creek and ERP, the larger drainage area and lower

422    proportion of forest coverage means that the streamflow was much higher within the ERP.

423

424    Figure 2: Discharge, and snow water equivalent throughout the study period (2016-2021). River

425    discharge (m s$^{-1}$) data depicts both the Coal Creek and ERP catchments. Snow water equivalent (m) is

426    derived from the SNOTEL station (Site 380).

427
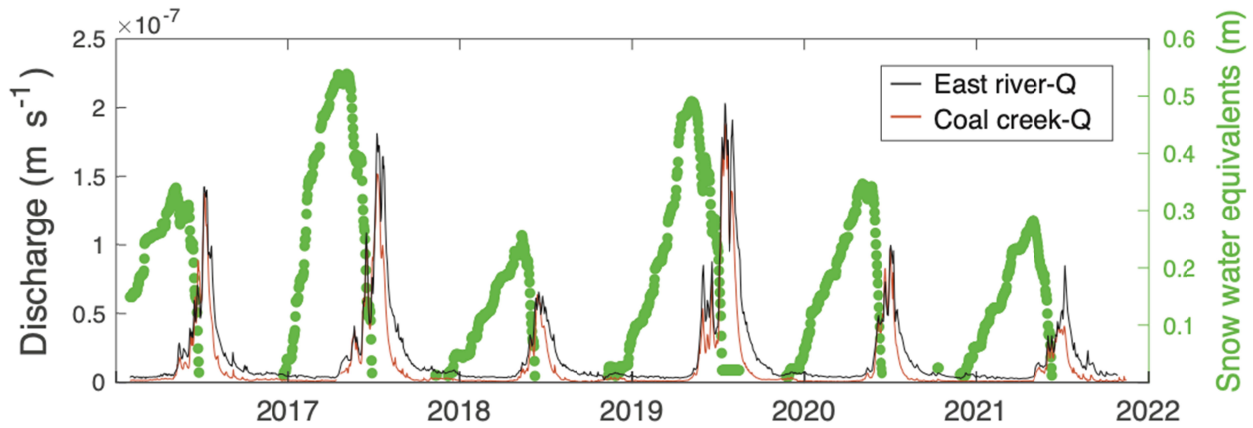
428
429

430    The magnitude of the annual average $NO_3^-$ export, after accounting for catchment areal extent

431    (Eq. 4 & 5), was higher within the ERP (1.71 Mg ± 1.2) relative to Coal Creek (0.3 Mg ± 0.13)

432    (Table 1 & Fig. S2). The pulse-shunt associated with snowmelt is responsible for the bulk of

433    solute export, accounting for 80-90% and 50-90 % of total $NO_3^-$ export in both Coal Creek and

434    ERP, respectively. The riverine $NO_3^-$ concentrations spanned a similar order of magnitude within

435    both the Coal Creek and ERP (Fig. 3a), and exhibited an overall chemostatic relationship with

436    discharge, showing minimal fluctuation under increasing discharge. However, slight differences

437    in cQ for $NO_3^-$ between Coal Creek and ERP are noted at intermediate discharge, whereby export

438    at ERP is slightly diluted, while Coal Creek is concentrated (Fig. 3a, i). The trends in $CV_c/CV_q$

439    support the highly variable nature of the cQ data for $NO_3^-$ (Fig. 3b), however, using this

440    approach, both catchments show evidence of chemodynamic behavior ($CV_c/CV_q > 1$). When

441    considered as independent water years (2016 - 2021), Coal Creek shows more conservative

442    behavior, with two years of overall chemostasis and the remainder chemodynamic. The strongest

443    chemodynamic regimes occur during the driest years (2018 and 2020). The $CV_c/CV_q$ for the ERP

444    showed stronger positive chemodynamic behavior across multiple years relative to Coal Creek,

445    in contrast to the cQ data. For both Coal Creek and ERP, this analysis shows the importance of

446    heterogeneous sources contributing to the aggregate export signal at different times of the year.

447

448    Table 1: Annual nitrate export magnitudes between East River and Coal Creek. These
449    calculations use gap-filled data, and are expressed as a function of the size of each watershed.
450    Annual $NO_3^-$ flux (Mg-megagrams) is calculated from Equation 4 at the water year time scale. Q
451    yield ($km^3$) is the total volume of water that exited the watershed for each water year. Atm. $NO_3^-$
452    deposition (Mg) is the total (i.e., wet + dry) nitrate deposition (kg-N/ha), summed across each
453    watershed area.

| | | 2016 | 2017 | 2018 | 2019 | 2020 | 2021 |
|---|---|---|---|---|---|---|---|
| **East River** | Annual $NO_3^-$ export (Mg) | 3.8 | 1.1 | 0.6 | 2.8 | 1.2 | 1.2 |
| | Q Yield $(km^3)$ | 0.05 | 0.07 | 0.03 | 0.09 | 0.04 | 0.03 |
| | Atm. $NO_3^-$ deposition (Mg) | 8.6 | 9.1 | 7.3 | 6.4 | 7.3 | 8.4 |
| **Coal Creek** | $NO_3^-$ annual export (Mg) | 0.3 | 0.3 | 0.1 | 0.5 | 0.3 | 0.3 |
| | Q Yield $(km^3)$ | 0.02 | 0.03 | 0.01 | 0.03 | 0.02 | 0.01 |
| | Atm. $NO_3^-$ deposition (Mg) | 6.4 | 6.5 | 5.3 | 4.9 | 5.3 | 6.1 |

454
455
456 Figure 3: (a) Concentration-discharge relationships for different solutes within the ERP and Coal
457 Creek catchments (i) nitrate, (ii) dissolved total nitrogen, (iii) chloride, and (iv) magnesium. Also
458 shown are the lines of best fit, the slope of which is represented in the powerlaw relationship as
459 exponent $b$ ($c=aQ^b$). (b) The ratio between the coefficient of variation for solute concentration
460 and discharge ($CV_c/CV_q$) plotted against the exponent ($b$) of the powerlaw relationship for the
461 same solutes as in (a). Each plot depicts the entirety of the data for the two watersheds (larger
462 points with solid black outline) and the data for each water year. Also depicted in these plots are
463 the positive and negative linear relationship between $CV_c/CV_q$ and $b$ (solid black lines), and the
464 threshold point (at $CV_c/CV_q = 0.5$, dotted line) separating chemostatic from chemodynamic
465 regimes.
466
467 Distinct relationships emerge during the rising and falling limb (Fig. 4, & Table 2). The rising
468 limb has little impact on riverine $NO_3^-$ in either the ERP ($b = 0.05$), or Coal Creek ($b = 0.1$).
469 However, the falling limb of the snowmelt period flushes $NO_3^-$ into the ERP ($b = -0.6$), as the

470 groundwater table reaches into the shallower soils. This impact is much weaker in Coal Creek ($b$

471 = -0.06). `

472

473 Figure 4: Relationship between the concentration of different nitrogen species ($NO_3^-$, DON),

474 chloride, and magnesium, relative to the discharge for (a) the East River catchment, and (b) Coal

475 Creek. The hydrograph is divided into the rising limb (increasing during the annual snowmelt

476 period), and the falling limb (decreasing to baseflow).

477
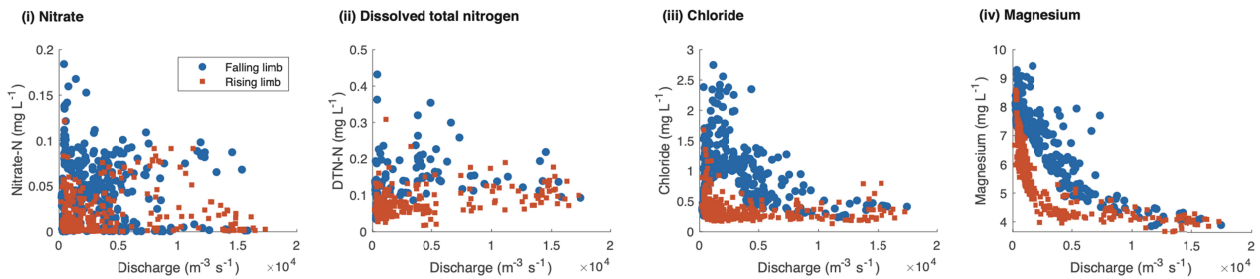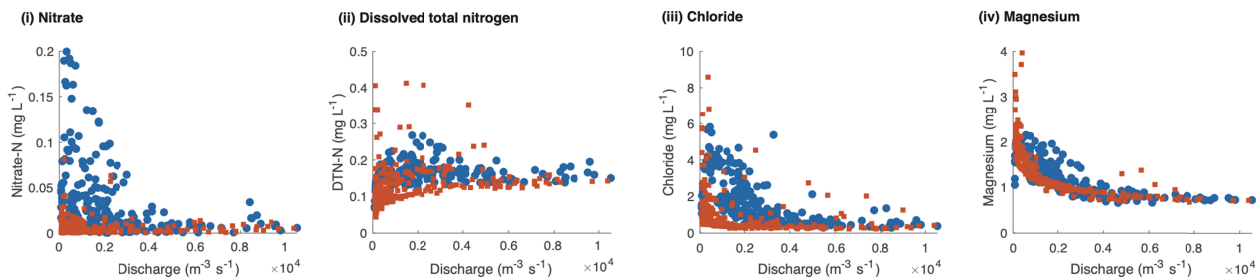


478
479
480 DTN showed a different relationship with Q than $NO_3^-$, which, given that riverine $NH_4^+$ was

481 extremely low (generally non-detectable, and always < 1 µM), likely reflects the export of

482 dissolved organic nitrogen in these systems. Within both catchments, DTN export increased with

483 increasing Q (Fig. 3a), which was stronger in Coal Creek ($b$ = 0.16) relative to ERP ($b$ = 0.07).

484 This relationship was also apparent under the falling limb in the ERP, and under increasing and

485 decreasing Q in Coal Creek (Table 2). The $CV_c/CV_q$ ratio was typically low (<0.5) for both Coal

486 Creek and the ERP, indicating that the variability in DTN export is strongly related to the

487 variation in discharge.

488

489 Table 2: Exponent $b$ for the concentration-discharge of various elements. The table provides the

490 value calculated from the complete dataset. In brackets are the ranges in $b$ spanned by individual

491    years (2016 - 2021), followed by the *b* values during the rising limb and the falling limb of the
492    hydrograph.
493
494

|  | East River | Coal Creek |
|---|---|---|
| **Nitrate** | 0.013 (-0.06/ 0.38\| 0.05/ -0.6) | -0.01 (-0.23/ -0.2\| 0.1/ -0.06) |
| **Dissolved total nitrogen** | 0.07 (-0.02/ 0.37\| 0.16/ 0.08) | 0.16 (0.11/ 0.2\| 0.14/ 0.2) |
| **Chloride** | -0.02 (-0.08/ 0.19\| -0.03/ -0.5) | -0.07 (-0.3/ 0.12\| -0.11/ -0.3) |
| **Magnesium** | -0.14 (-0.18/ 0\| -0.15/ -0.24 ) | -0.26 (-0.3/ -0.21\| -0.17/ 0.25) |

495

496    Chloride export was measured as a conservative tracer of watershed export processes, and

497    showed a broad chemostatic relationship with Q in ERP (*b* = -0.02, with an interannual range = -

498    0.08 - 0.19), and a slightly stronger dilution of Cl concentration within increasing Q in Coal

499    Creek (*b* = -0.07, interannual range = -0.3 - 0.12) and ERP. The cQ relationship for magnesium

500    provides insight into the export behavior of a predominantly bedrock-derived solute. Riverine

501    Mg concentration was far higher in the ERP where soils are underlain by a Cretaceous Mancos

502    shale bedrock, however, the trajectory of Mg export was similar between the catchments and

503    generally showed a non-linear decline in concentration under increasing Q (Fig. 3a, 4). $CV_c/CV_q$

504    ratios generally underlie the observations from cQ slopes, with groundwater, and geogenically-

505    derived solutes showing little variability in concentrations, and are strongly driven by changes in

506    discharge (Fox et al., 2022).

507

508    Causality analyses (performed using transfer entropy, (Ruddell & Kumar, 2009) was used to

509    further parse out the factors regulating $NO_3^-$ transit and export (Fig. S3a/b). SWE and water

510    temperature were important factors governing $NO_3^-$ export from both catchments (Fig. S3c).

511    However, both biogenic and geogenic variables were closely associated with $NO_3^-$ release to

512    streams within the ERP, indicating the contribution of both shallow and deep sources to the $NO_3^-$

513    aggregate flux. By contrast, $NO_3^-$ exported from Coal Creek showed no direct connection to

514    biogenic or geogenic export (Fig. S3c), indicating the strong role atmospheric deposition plays in

515    contributing to $NO_3^-$ export.

516

517  *3.2. Streamwater $\delta^{15}N_{NO3}$ and $\delta^{18}O_{NO3}$:* The isotopic composition of $NO_3^-$ ($\delta^{15}N_{NO3}$ and $\delta^{18}O_{NO3}$)

518  in stream water within Coal Creek and the ERP was measured across a two-year period between

519  2019 to 2021, capturing historic highs and lows in snowpack depth and streamflow (Fig. 5a). The

520  lower $NO_3^-$ concentrations within Coal Creek (< 2 µM) precluded isotopic measurements during

521  much of the baseflow period, and measurements focused mainly on the snowmelt period (Fig.

522  5a). The $\delta^{15}N_{NO3}$ within the ERP showed a narrower range of values than Coal Creek. In the ERP

523  $\delta^{15}N_{NO3}$ spanned -2.3 - 19.2 ‰ (3.8 ± 4.4 ‰, mean and standard deviation), and 1.4 - 24 ‰ (8.9

524  ± 6 ‰) in Coal Creek.  Similarly, $\delta^{18}O_{NO3}$ ranged from 1.2 to 27.8 ‰ (11.8 ± 6.8 ‰) in the ERP,

525  and 1.5 - 44.5 ‰ (19.3 ± 7.3 ‰) in Coal Creek (Fig. 5b).

526

527  Figure 5: River concentration and isotope data for the (a) ERP, and (b) Coal Creek. Subplots a

528  and b are divided into three panels, depicting the river nitrate concentrations (top panel), $^{15}N_{NO3}$

529  (middle panel), and $^{18}O_{NO3}$ (bottom panel). Panel (c) depicts the relationships between

530  $^{15}N_{NO3}/^{18}O_{NO3}$ within streamwater collected within Coal Creek and the ERP.

531
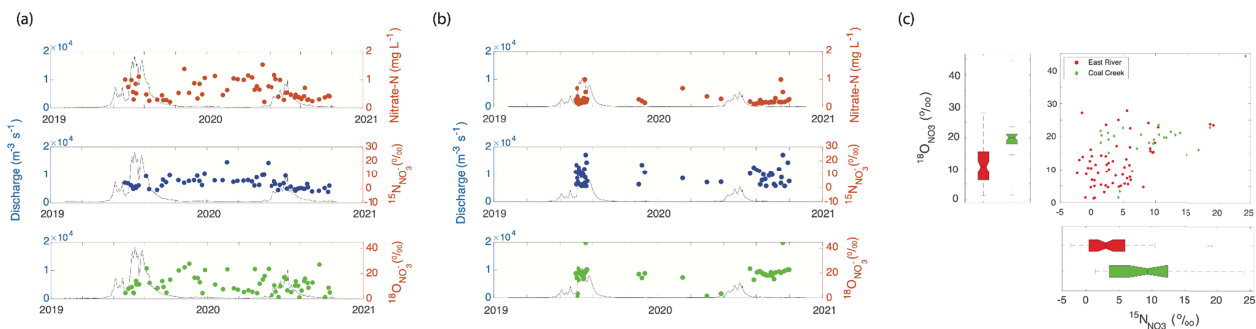


532
533
534

535  *3.3. Sources of exported nitrate:* We used a simple two-end member mixing model to determine

536  the contributions of atmospheric and soil-/ saprolite-derived $NO_3^-$ to aggregate $NO_3^-$ export. The

537  atmospheric component of this mixing model was derived from measurements of the isotopic

538  composition of precipitation from both Coal Creek and ERP. The isotopic signal of both snow

539  and rainfall overlapped between the two catchments, showing an average (± standard deviation)

540  $\delta^{15}N_{NO3}$ of 6.4 ± 4.3 ‰ and 18.6 ± 5 ‰ and a $\delta^{18}O_{NO3}$ average of 73 ± 11.1 ‰ and 65.6 ± 9.6 ‰,

541  for rainfall and snowfall respectively (Fig. S4). The soil-derived signal is attributable to

542  nitrification, and is calculated from a $\delta^{18}O$ value of $O_2$, and measured values of $\delta^{18}O$ for

543  porewater from the hillslope boreholes. The specific approach for estimating the $\delta^{18}O$ values of

544  nitrification can be found in the supplemental material and methods. Measurements of dissolved

545    $NO_3^-$ were not made for Coal Creek soils, so mixing model calculations were made using

546    nitrification data derived from ERP soils, which overlap with previously published values

547    (Granger & Wankel, 2016). This mixing model demonstrated that a larger fraction of riverine

548    $NO_3^-$ exported from Coal Creek was derived directly from atmospheric deposition (~41 %), with

549    the remainder sourced from soil pools. The range of atmospheric contributions to $NO_3^-$ export in

550    Coal Creek varied from 20 to 62 % (Table S1). A weighted approach to calculating percent

551    contribution of atmospheric sources to distinct periods of the hydrograph shows it to be larger

552    during the snowmelt period (34 ± 5 %) relative to baseflow (20 ± 4 %) (Table S2). By contrast,

553    the majority of exported $NO_3^-$ from the ERP was derived from nitrification (~82 %), with a

554    smaller direct contribution from atmospheric $NO_3^-$ deposition, ranging across the year from 16 to

555    29 %. A biplot depicting $\delta^{18}O_{NO3}$ and $\delta^{15}N_{NO3}$ suggests that the groundwater accumulating within

556    toeslopes, and from $NO_3^-$ the floodplain were significant sources of ERP riverine $NO_3^-$ (Fig. S4).

557    Finally, the ERP showed a relatively high range of $\delta^{18}O_{NO3}$ throughout the year, however, the

558    percent contribution of atmospheric $NO_3^-$ to export was similar during the snowmelt period (22 ±

559    3 %), and baseflow (24 ± 7 %) (Table S2).

560

561    Periodically, the $NO_3^-$ isotope time series within ERP showed concomitant enrichment of both

562    $\Delta\delta^{18}O_{NO3}: \Delta\delta^{15}N_{NO3}$ (Fig. 5a, c). These periods occur during snowmelt and under baseflow

563    conditions, albeit with slightly different enrichment relationships between the two isotopes, of

564    1.2 and 0.6 during snowmelt and baseflow respectively (Fig. S5). These periods suggest an

565    actively fractionating mechanism (e.g., denitrification) is contributing to $NO_3^-$ loss from solution.

566    By contrast, evidence for strongly fractionating loss pathways within Coal Creek were not

567    observed.

568

569    *3.4. Terrestrial nitrate cycling in the East River:* To strengthen our understanding of how

570    different sources and sinks contribute to the aggregate $NO_3^-$ export within the ERP catchment, we

571    developed a depth-resolved, time series of $\delta^{15}N_{NO3}$ and $\delta^{18}O_{NO3}$ across a hillslope-toeslope-

572    floodplain transect. This time series permits the identification of major source-sink hotspots

573    across the terrestrial system that likely account for the stronger biogeochemical processing of

574    nitrogen within the ERP. Moreover, the time period of intensive sampling encompassed the same

575    event driven trajectory as the riverine data, capturing historic high and low snowpack depths,

576   which dictated much of the variance in water table depth, and runoff. Across this transect, the

577   $\delta^{15}N_{NO3}$ and $\delta^{18}O_{NO3}$ spanned a large range indicative of multiple sources contributing to nitrate

578   accumulation and cycling (Fig. 6a, S6a). Within shallower soil horizons, $\delta^{15}N_{NO3}$ and $\delta^{18}O_{NO3}$

579   ranged from -7.5 to 19 ‰ and -10.5 to 21 ‰, respectively. Within the shale weathering zone

580   $\delta^{15}N_{NO3}$ ranged from ~ 1 ‰ to 20 ‰, and $\delta^{18}O_{NO3}$ from -10 ‰ to 14 ‰. The fractured bedrock

581   showed a range in $\delta^{15}N_{NO3}$ from ~ -5 ‰ to 8 ‰, and -29 ‰ to 22 ‰ for $\delta^{18}O_{NO3}$.

582   A simple mixing model was used to calculate the contribution of atmospheric deposition to

583   subsurface $NO_3^-$ pools across depth and time. Broadly, percent atmospheric $NO_3^-$ increased with

584   depth from 12 % (range: 1.1 - 41 %) within shallow soil layers to 20.2 % (0 - 43.4 %) within the

585   fractured bedrock, with the saprolite weathering zone showing intermediate levels of

586   atmospheric $NO_3^-$ (~14 %: 4 - 33 %. Table S1, Fig. S6a). Contribution of atmospheric $NO_3^-$ to

587   $NO_3^-$ pools increased during the snowmelt period (Fig. S6b) within the shallow soils, but

588   particularly in saprolite weathering zone, where the contribution increased to ~21 %, with an

589   upper range of ~32%. This contribution dropped under baseflow conditions (~9 %).

590   The trajectory of the $\Delta\delta^{18}O_{NO3}$: $\Delta\delta^{15}N_{NO3}$ showed distinct relationships across the different

591   regions of the soil profile (Fig. 6b). The shallow soil horizon showed a weak relationship

592   between $\Delta\delta^{18}O_{NO3}$: $\Delta\delta^{15}N_{NO3}$ of ~ 0.06. However, both the weathering zone and the fractured

593   bedrock showed stronger $\Delta\delta^{18}O_{NO3}$: $\Delta\delta^{15}N_{NO3}$ relationships of ~ 0.7 and 0.5, respectively. The

594   weathering zone, which shows the strongest $\Delta\delta^{18}O_{NO3}$: $\Delta\delta^{15}N_{NO3}$ trajectory, shows a clear

595   combination of both mixing processes, and fractionating processes (e.g., nitrate reduction, nitrate

596   reoxidation). However, approximately 25 - 30 % of the nitrate in weathering zone originated

597   from atmospheric deposition (which imparts a high $\delta^{18}O_{NO3}$ value), precluding the identification

598   of any one process dominating $NO_3^-$ dynamics and demonstrating this zone to be a strong

599   integrator of different $NO_3^-$ sources.

600

601   Figure 6: Relationships between $^{15}N_{NO3}/^{18}O_{NO3}$ within the terrestrial zone, (a) $^{15}N_{NO3}/^{18}O_{NO3}$
602   across different soil depths on the hillslope (i.e., Shallow soil horizon, weathering zone, and
603   consolidated bedrock). The correlation between the $^{15}N_{NO3}/^{18}O_{NO}$ measurements are provided in
604   brackets in each legend. (b) The same relationship within two different depths (i.e., shallow soil
605   horizon, and saprolite weathering zone,) at different points along the transect encompassing the
606   upper- and mid-hillslope, and the toeslope. As for panel a, the value in brackets represents the
607   correlation between the $^{15}N_{NO3}/^{18}O_{NO}$.

608

609
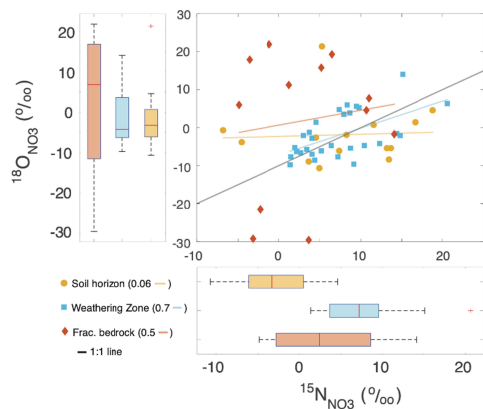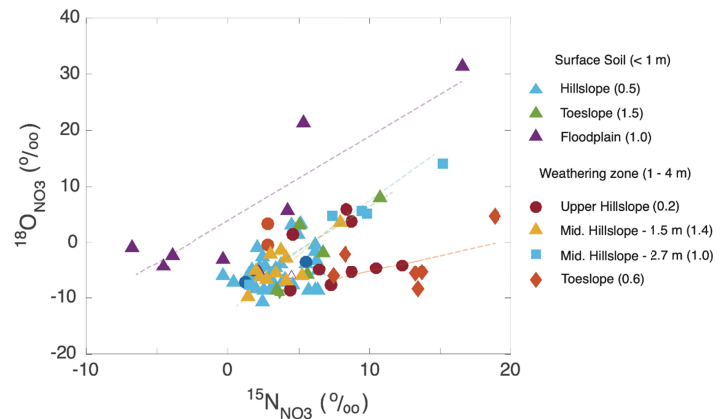
The $\Delta\delta^{18}O_{NO3}$: $\Delta\delta^{15}N_{NO3}$ relationship also showed clear variability across the hillslope-toeslope-floodplain transect that was related to water residence time. Regions with long transit times, i.e., within shallower soils at the floodplain, and the weathering zone (~2.7 m depth) at the hillslope, showed a concomitant enrichment between $\Delta\delta^{18}O_{NO3}$: $\Delta\delta^{15}N_{NO3}$ (Fig. 6b), which is indicative of an actively fractionating mechanism (e.g., denitrification). The shallow soils at the toeslope, and the soil-saprolite transition zone at the mid-hillslope (~1 m) had a slightly higher relationship between $\Delta\delta^{18}O_{NO3}$: $\Delta\delta^{15}N_{NO3}$ of 1.5. Finally, the regions with slightly faster transit times, i.e., shallow soils on the hillslope where soil moisture increases briefly with snowmelt as the water table rise, or the weathering zone of the toeslope, both show a lower $\Delta\delta^{18}O_{NO3}$: $\Delta\delta^{15}N_{NO3}$ ratio of 0.6, which implies both source water mixing and *in situ* transformation occurs in this region.

**4. Discussion**

Gradients in vegetation, topography, geology, and geomorphology all play critical roles in determining nitrogen availability, and regulating its retention and release from mountainous headwaters (Bormann & Likens, 1967; Sebestyen et al., 2014, 2019). Paired catchment studies are important approaches to improve understanding of the role distinct geophysical and ecological traits play in the transformation of nitrogen while controlling for climatic properties, and the magnitude of nitrogen deposition.

630    When normalized to catchment area, the East River at pumphouse (ERP) exported between 3 to

631    12x as much $NO_3^-$ as Coal Creek (Table 1 & Fig. 8). The ERP is the larger catchment and nitrate

632    deposition is calculated to be a little higher ($7.8 \pm 1$ MG in ERP, relative to $5.7 \pm 0.7$ MG in Coal

633    Creek). Both catchments show large variability in $NO_3^-$ concentrations across the measured range

634    in discharge (Fig. 3a/b), indicating the contribution of multiple sources of terrestrial $NO_3^-$ to the

635    aggregate downstream export profile (Thompson et al., 2011). A causality analysis illustrates

636    both similarities in the main factors driving $NO_3^-$ export between the two catchments (e.g., the

637    considerable influence of SWE), but also clear distinctions. For example, $NO_3^-$ export in the ERP

638    is more strongly related to biogenic (e.g., microbial turnover of DOC, which can be tied to $NO_3^-$

639    reduction) and geogenic (e.g., bedrock weathering) processes (Fig. S3), implying a more

640    complex role of shallow and deep sources of $NO_3^-$ in the ERP (Zhi & Li, 2020). By contrast,

641    nitrate export in Coal Creek showed little information transfer between biogenic and geogenic

642    processes, suggesting little microbial transformation prior to export, and no contribtion of

643    bedrock weathering to $NO_3^-$ export. In the following sections we discuss the role of vegetation,

644    redox heterogeneity, and bedrock properties in contributing to differences in the retention and

645    release of $NO_3^-$ between the two catchments.

646

647    Figure 7: Schematic representation of different retention of $NO_3^-$ (in megagrams, MG) across the
648    two catchments as a function of their distinct vegetation and bedrock properties. Also provided
649    are the direct contribution of atmospherically deposited nitrate ($N^{18}O_3^{ATM}$) to exported $NO_3^-$, and
650    the % of atmospherically deposited $NO_3^-$ retained in different watersheds. Estimates of the
651    contribution of bedrock weathering are also provided for ERP. The units for the different fluxes
652    are in megagrams (MG), and are normalized to the individual catchment size.
653
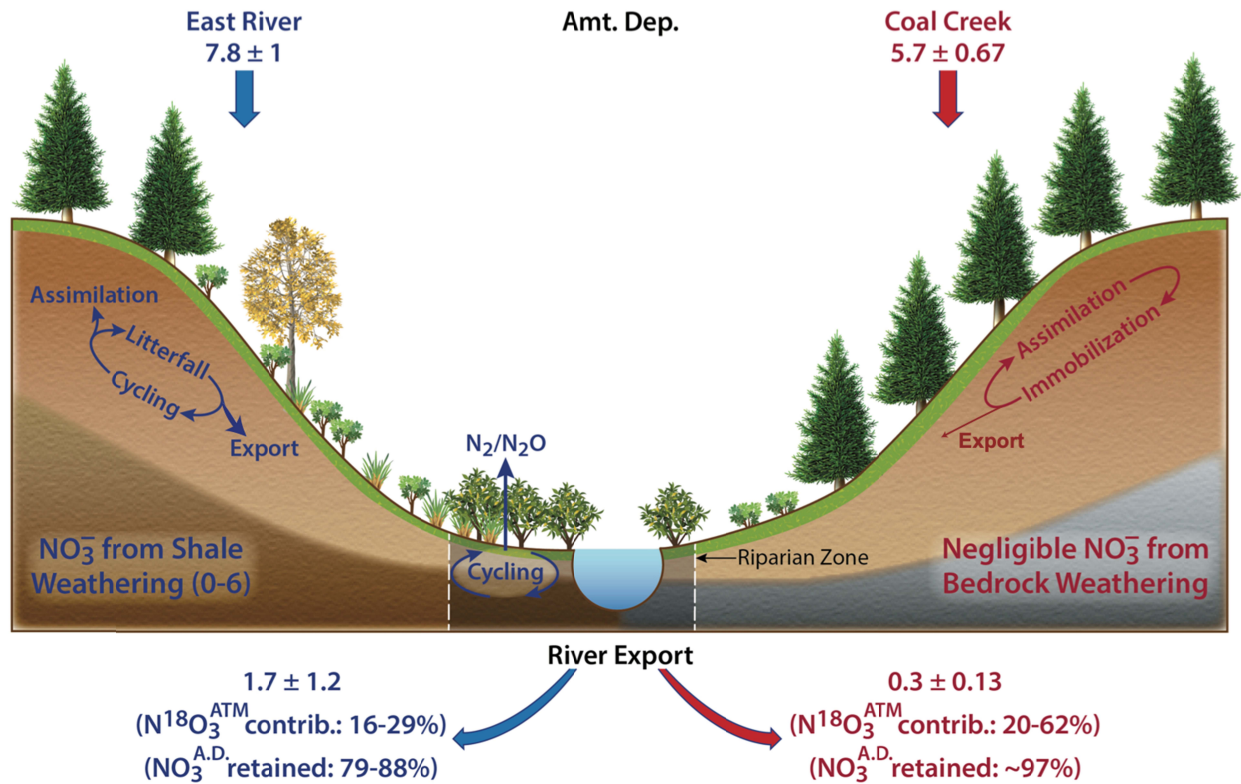
East River
7.8 ± 1

Amt. Dep.

Coal Creek
5.7 ± 0.67

Assimilation
Litterfall
Cycling
Export

$N_2/N_2O$

Assimilation
Immobilization
Export

$NO_3^-$ from Shale Weathering (0-6)

Cycling

Riparian Zone

Negligible $NO_3^-$ from Bedrock Weathering

River Export

1.7 ± 1.2
($N^{18}O_3^{ATM}$ contrib.: 16-29%)
($NO_3^{A.D.}$ retained: 79-88%)

0.3 ± 0.13
($N^{18}O_3^{ATM}$ contrib.: 20-62%)
($NO_3^{A.D.}$ retained: ~97%)

EESA23-010

*4.1. Vegetation controls on $NO_3^-$ cycling:* The contrasting vegetation distributions between Coal Creek and ERP likely play a large role in the retention and release of $NO_3^-$ at the catchment scale. Coal Creek is dominated by coniferous forests (predominantly *Picea engelmannii* and *Abies lasiocarpa*), while ERP has a more heterogeneous land cover, with extensive regions of barren alpine and subalpine land, mixed forest, and shrub and grassland. The strong forest coverage of Coal Creek can give rise to efficient and closed nitrogen cycles (Fahey et al., 1985; Gosz, 1981), where the turnover (depolymerization and mineralization) of soil nitrogen pools, and recycling of internal pools sustains nitrogen demand, and reduces $NO_3^-$ export from the catchment (Fig. 8). Moreover, plant traits associated with conifers, including a higher leaf mass area and lower nitrogen content in litter, would further nitrogen turnover and loss. Further supporting this idea of higher retention in forested catchments, a recent study (Gurmesa et al., 2022) demonstrated strong assimilation of $NO_3^-$, relative to $NH_4^+$, by plants on a global scale, contrary to expectations for inorganic nitrogen assimilation based upon the energetic costs of assimilating reduced compounds (Kronzucker et al., 1997). Furthermore, low $NO_3^-$ concentrations within Coal Creek (Table 1 & Fig. 8) may stem from immobilization of nitrogen

24

672    by bacteria and fungi during the decomposition of woody debris following tree mortality.

673    Previous studies have attributed the net retention in forested watersheds, and subsequent declines

674    in $NO_3^-$ export, to the accumulation of high C: N woody debris, and immobilization of dissolved

675    nitrogen (Lajtha, 2020). Preliminary work has shown a higher mortality rate amongst conifers

676    within Coal Creek relative to the ERP (Falco et al., in prep.), which could contribute to the

677    disparity in retention between the two catchments.

678

679    The vegetation in ERP includes montane species (e.g., *Artemisia spp.* and *Festuca spp.*), Aspen

680    glades (*Populus tremuloides*), and conifer stands (*Picea engelmannii, and Abies lasiocarpa*), that

681    likely lead to a more open nitrogen cycle, particularly through litter accumulation and turnover

682    (Maavara et al., 2021). The difference in vegetation communities between the two catchments

683    also contributes to distinct hydrological cycles, which play a critical role in nitrogen cycling and

684    solute export (Webb et al., 2020; Woelber et al., 2018). The dense forest coverage within Coal

685    Creek increases the loss of snow via canopy interception, ablation, and evapotranspiration,

686    reducing that contributing to river flow (Fig. 2) (Sprenger et al., 2022). A higher rate of ET can

687    lower the depth of the groundwater table (Condon et al., 2020), reducing connectivity between

688    hillslopes and the river, increasing nitrogen retention in upslope regions of Coal Creek.

689

690    *4.2. Bedrock properties and nitrogen cycling:* A further fundamental difference between Coal

691    Creek and ERP concerns the underlying bedrock. The ERP is largely underlain by nitrogen-rich

692    Mancos Shale bedrock, which has been previously reported to show high rates of weathering as

693    snowmelt-driven groundwaters rise and fall (Wan et al., 2019, 2020; Winnick et al., 2017). Wan

694    et al., (Wan et al., 2020) estimated a base cation weathering rate for a hillslope within the ERP of

695    $55.3 \pm 4$ $Kmol_c$ $ha^{-1}$ $yr^{-1}$, and a shale-nitrogen release rate of $18.9 \pm 4.4$ kg $ha^{-1}$ $yr^{-1}$, and a specific

696    hillslope $NO_3^-$ export of ~2.0 kg $ha^{-1}$ $yr^{-1}$. The bulk of this exported $NO_3^-$ is likely assimilated by

697    plants or reduced by microbes within the floodplain (see discussion below), therefore, the

698    contribution of geogenic sources of $NO_3^-$ to the aggregate export signal remains uncertain. Water

699    table depths dominate solute transport to the river, and shape the characteristic cQ relationships

700    for different solutes. Zhi et al., formally described how distinct solute sources govern water

701    chemistry within Coal Creek, demonstrating that low water table depths under baseflow

702    conditions, or during particularly dry years, activate organic-poor, geogenic sources of solutes

703  (Zhi et al., 2019). The relationship between Mg and discharge replicates this dilution pattern
704  within both catchments (Fig. 3a,b). However, $NO_3^-$ demonstrates strong variability with stream
705  discharge (Fig. 3a). Incidences of high $NO_3^-$ export under baseflow conditions could represent
706  the contribution of geogenic sources in the ERP, however, the variability in cQ is similar to that
707  in Coal Creek (Fig. 3a, b), which is underlain by crystalline igneous rocks containing only trace
708  amounts of nitrogen Holloway & Dahlgren, 2002). The high $NO_3^-$ concentrations exported under
709  low discharge in both catchments likely reflects the legacy storage, and subsequent mobilization,
710  of groundwater $NO_3^-$ (Johnson & Stets, 2020), which is contributed to by bedrock weathering in
711  the ERP (Wan et al., 2020).
712
713  Estimating the contribution of bedrock $NO_3^-$ to exports is further complicated by the variability
714  in the extent of bedrock weathering (and nitrogen release) throughout the ERP catchment,
715  particularly with aspect and the degree of infiltration (Pelletier et al., 2018). The northeast-facing
716  hillslope, where the bulk of our data is derived, shows high fracture density and a high
717  weathering rate. There is, however, considerable variability in the weathering potential of the
718  Mancos shale throughout the ERP, with areas towards the headwaters of the catchment underlain
719  by older, harder shale, with fewer fractures through the shale (discussed further in Maavara et al.,
720  2021). We therefore consider that at the catchment scale, bedrock nitrogen from the hillslope
721  contributes significantly less to watershed $NO_3^-$ export than it likely does to floodplain nitrogen
722  cycling, and, as such, assume a value between 0 - 1 kg ha$^{-1}$ yr$^{-1}$ for our estimate of catchment
723  export (Fig. 8). After accounting for this potential contribution of bedrock weathering to $NO_3^-$
724  export, Coal Creek shows a significantly higher retention of $NO_3^-$ relative to the ERP. We
725  estimate that approximately 97 % of deposited $NO_3^-$ is retained in Coal Creek, relative to ~78-88
726  % in the ERP.
727
728  *4.3. Riparian contributions to $NO_3^-$ retention:* Coal Creek and the ERP differ further in
729  geomorphology, with the ERP showing much higher sinuosity through the valley and a larger
730  areal extent of the riparian region. These are important features regulating the sources of
731  exported $NO_3^-$. The majority of $NO_3^-$ exported by watersheds tends to be derived close to the
732  river (Sebestyen et al., 2019). A smaller riparian region within Coal Creek reduces preprocessing
733  of that $NO_3^-$ prior to export, which might account for the higher contribution of atmospheric

734   sources of $NO_3^-$ to aggregate export (Fig. 5). This contribution increases during the snowmelt

735   period (Table S2), consistent with previous analyses partitioning contributions to aggregate $NO_3^-$

736   export (Sebestyen et al., 2019), and likely attributable to rapid transit times, and fewer

737   opportunities for biological transformations during the snowmelt period.

738

739   The ERP shows a higher variability in the sources of $NO_3^-$ contributing to its aggregate export

740   (Fig. 5a). The mobilization of soil-derived $NO_3^-$ during snowmelt results in a chemodynamic

741   relationship with streamflow (Fig. 3b), and increasing export under the rising and falling limb of

742   snowmelt (Fig. 4a). Across the year, the exported $NO_3^-$ has a distinct isotopic composition from

743   the terrestrial sources. For example, the contribution of atmospheric $NO_3^-$ to terrestrial pools

744   shows a strong interannual pattern, increasing during the snowmelt period, and declining during

745   baseflow (Fig. S6b). This pattern is not reflected in the river $NO_3^-$ isotopic signal (Fig. 5a, &

746   Table S2), reflecting the contribution of different ecosystem control points, particularly, the

747   overriding impact of critical zone and floodplain processes. The fluctuating water table also

748   prolongs transit times and reactivity within the critical zone, and the riparian region. This

749   promotes the formation of strong oxic/anoxic gradients, and the spatial and temporal coupling of

750   aerobic (e.g., nitrifying) and anaerobic (denitrifying) metabolisms (Bouskill et al., 2019). A mass

751   balance calculation using subsurface $NO_3^-$ cQ from the upper hillslope region to the toeslope

752   suggests that much of the $NO_3^-$ accumulating within the hillslope critical zone is subject to

753   denitrification prior to export (Wan et al., 2020). Further support for this mechanism of loss

754   comes from our observations of very low to undetectable $NO_3^-$ concentrations within riparian

755   regions in ERP and the isotopic enrichment of $NO_3^-$ (Fig. S4), along a $\Delta\delta^{18}O_{NO3}: \Delta\delta^{15}N_{NO3}$

756   trajectory of 0.6 (Fig. 7), indicative of actively fractionating mechanisms (e.g., nitrite oxidation

757   and denitrification, Granger & Wankel, 2016).

758

759   The functional potential for denitrification was observed across the ERP riparian region

760   (Carnevali et al., 2020), however, this area was also been shown to be a potential hotspot for

761   DNRA (Carnevali et al., 2020), which fractionates the $^{15}N$ and $^{18}O$ of $NO_3^-$ in a similar manner

762   ($^{15}\varepsilon:^{18}\varepsilon = 0.5 - 1.0$) to denitrifying bacteria (Asamoto et al., 2021). Rogers et al., modeled the

763   hydrological and biogeochemical processes retaining and releasing nitrogen within the ERP

764   riparian region, concluding that these regions are major control points for river corridors,

765    providing ~20 % of the stream $NO_3^-$, but remaining major sinks for $NO_3^-$, due to a combination

766    of denitrification and dissimilatory nitrate reduction to ammonium (DNRA) (Rogers et al.,

767    2021). Under certain conditions, DNRA and denitrification co-exist (Jia et al., 2020), however,

768    their environmental impact is distinct. At the ecosystem scale DNRA tends to function as an

769    ecosystem retention mechanism for nitrogen, which might be important in nitrogen limited

770    ecosystems.

771

772    **5. Conclusions**

773

774    Nitrogen retention plays a critical role in ecosystem function in mountainous watersheds.

775    However, the nitrogen cycle is undergoing substantial perturbation (Steffen et al., 2015), and the

776    reported onset of oligotrophication of the nitrogen cycle in undisturbed catchments (Craine et al.,

777    2018; Mason et al., 2022), can undermine watershed function under future warmer and drier

778    climate scenarios predicted to disturb mountainous ecosystems (Siirila-Woodburn et al., 2021).

779    Predicting how this disturbance might feedback onto watershed function can be improved by

780    viewing function through the lens of watershed traits (McDonnell et al., 2007), which is

781    emphasized by the current paired catchment approach. Watershed traits, including topography,

782    bedrock weathering properties, soil properties, land cover, etc., are emergent features of the

783    historical climate, and regulate the storage and release of water and solutes between different

784    catchments.  Improving our understanding of whether analagous assemblages of traits retain and

785    release solutes in comparable ways (i.e., whether conifer dominated forests through the Rocky

786    Mountains retain atmospheric nitrate and release a larger share of unprocessed nitrate) would

787    allow these catchments, and their potential response to disturbance, to be considered together in

788    regional scale models. This study also demonstrates the importance of integrating common

789    measurements, such as cQ analysis, with stable isotope measurements of $NO_3^-$, to improve

790    understanding of how catchments with similar cQ relationships can differ strongly in their

791    nitrogen cycles.

792

796

**Data availability:** The data and scripts used to produce the figures are available publicly through

https://data.ess-dive.lbl.gov/data via doi:10.15485/1660462, doi:10.15485/1660456. While

streamflow and discharge data are available at doi:10.15485/1779721, and

doi:10.21952/WTR/1495380.

801

**References**

803

Alexander, R. B., Boyer, E. W., Smith, R. A., Schwarz, G. E., & Moore, R. B. (2007). The Role

of Headwater Streams in Downstream Water Quality1: The Role of Headwater Streams

in Downstream Water Quality. *JAWRA Journal of the American Water Resources

Association*, *43*(1), 41–59. https://doi.org/10.1111/j.1752-1688.2007.00005.x

Asamoto, C. K., Rempfert, K. R., Luu, V. H., Younkin, A. D., & Kopf, S. H. (2021). Enzyme-

Specific Coupling of Oxygen and Nitrogen Isotope Fractionation of the Nap and Nar

Nitrate Reductases. *Environmental Science & Technology*, *55*(8), 5537–5546.

https://doi.org/10.1021/acs.est.0c07816

Ascott, M. J., Gooddy, D. C., Wang, L., Stuart, M. E., Lewis, M. A., Ward, R. S., & Binley, A.

M. (2017). Global patterns of nitrate storage in the vadose zone. *Nature Communications*,

*8*(1), 1416. https://doi.org/10.1038/s41467-017-01321-w

Bastian, M., Heymann, S., & Jacomy, M. (2009). Gephi: An Open Source Software for

Exploring and Manipulating Networks. *Proceedings of the International AAAI

Conference on Web and Social Media*, *3*(1), 361–362.

https://doi.org/10.1609/icwsm.v3i1.13937

Basu, N. B., Thompson, S. E., & Rao, P. S. C. (2011). Hydrologic and biogeochemical

functioning of intensively managed catchments: A synthesis of top-down analyses:

Managed catchments. *Water Resources Research*, *47*(10).

822 https://doi.org/10.1029/2011WR010800

823 Berhe, A. A., & Torn, M. S. (2017). Erosional redistribution of topsoil controls soil nitrogen

824  dynamics. *Biogeochemistry*, *132*(1–2), 37–54. https://doi.org/10.1007/s10533-016-0286-

825  5

826 Bormann, F. H., & Likens, G. E. (1967). Small watersheds can provide invaluable information

827  about terrestrial ecosystems., *155*, 7.

828 Bourgeois, I., Clément, J., Caillon, N., & Savarino, J. (2019). Foliar uptake of atmospheric

829  nitrate by two dominant subalpine plants: insights from *in situ* triple-isotope analysis.

830  *New Phytologist*, *223*(4), 1784–1794. https://doi.org/10.1111/nph.15761

831 Bouskill, N. J., Conrad, M. E., Bill, M., Brodie, E. L., Cheng, Y., Hobson, C., et al.

832  (2019). Evidence for Microbial Mediated $NO_3^-$ Cycling Within Floodplain

833  Sediments During Groundwater Fluctuations. *Frontiers in Earth Science*, *7*, 189.

834  https://doi.org/10.3389/feart.2019.00189

835 Brookshire, E. N. J., Valett, H. M., & Gerber, S. (2009). Maintenance of terrestrial nutrient loss

836  signatures during in-stream transport. *Ecology*, *90*(2), 293–299.

837  https://doi.org/10.1890/08-0949.1

838 Campbell, D. H., Kendall, C., Chang, C. C. Y., Silva, S. R., & Tonnessen, K. A. (2002).

839  Pathways for nitrate release from an alpine watershed: Determination using $\delta^{15}N$ and $\delta$

840  $^{18}O$: ALPINE WATERSHED NITRATE $\delta^{15}N$ AND $\delta^{18}O$. *Water Resources Research*,

841  *38*(5), 10-1-10–9. https://doi.org/10.1029/2001WR000294

842 Carnevali, P. B. M., Lavy, A., Thomas, A. D., Crits-Christoph, A., Diamond, S., Meéheust, R., et

843  al. (2020). *Meanders as a scaling motif for understanding of floodplain soil microbiome*

844        *and biogeochemical potential at the watershed scale* (preprint). Microbiology.

845        https://doi.org/10.1101/2020.05.14.086363

846  Carroll, R. W. H., Gochis, D., & Williams, K. H. (2020). Efficiency of the Summer Monsoon in

847        Generating Streamflow Within a Snow-Dominated Headwater Basin of the Colorado

848        River. *Geophysical Research Letters*, *47*(23). https://doi.org/10.1029/2020GL090856

849        Carroll, Rosemary, Newman, Alexander, Beutler, Curtis, and Williams, Kenneth. (2021).

850        Stream discharge data collected within the East River, Colorado for the Lawrence

851        Berkeley National Laboratory Watershed Function Science Focus Area (water years 2019

852        to 2020). doi:10.15485/1779721.

853  Casciotti, K. L., Sigman, D. M., Hastings, M. G., Böhlke, J. K., & Hilkert, A. (2002).

854        Measurement of the Oxygen Isotopic Composition of Nitrate in Seawater and Freshwater

855        Using the Denitrifier Method. *Analytical Chemistry*, *74*(19), 4905–4912.

856        https://doi.org/10.1021/ac020113w

857  Clark, S. C., Barnes, R. T., Oleksy, I. A., Baron, J. S., & Hastings, M. G. (2021). Persistent

858        Nitrate in Alpine Waters with Changing Atmospheric Deposition and Warming Trends.

859        *Environmental Science & Technology*, *55*(21), 14946–14956.

860        https://doi.org/10.1021/acs.est.1c02515

861  Condon, L. E., Atchley, A. L., & Maxwell, R. M. (2020). Evapotranspiration depletes

862        groundwater under warming over the contiguous United States. *Nature Communications*,

863        *11*(1), 873. https://doi.org/10.1038/s41467-020-14688-0

864  Craine, J. M., Elmore, A. J., Wang, L., Aranibar, J., Bauters, M., Boeckx, P., et al. (2018).

865        Isotopic evidence for oligotrophication of terrestrial ecosystems. *Nature Ecology &*

866        *Evolution*, *2*(11), 1735–1744. https://doi.org/10.1038/s41559-018-0694-0

867 Fahey, T. J., Yavitt, J. B., Pearson, J. A., & Knight, D. H. (1985). The nitrogen cycle in

868            lodgepole pine forests, southeastern Wyoming. *Biogeochemistry*, *1*(3), 257–275.

869            https://doi.org/10.1007/BF02187202

870 Finlay, R. D., Frostegard, A., & Sonnerfeldt, A.-M. (1992). Utilization of organic and inorganic

871            nitrogen sources by ectomycorrhizal fungi in pure culture and in symbiosis with Pinus

872            contorta Dougl. ex Loud. *New Phytologist*, *120*(1), 105–115.

873            https://doi.org/10.1111/j.1469-8137.1992.tb01063.x

874 Fox, P. M., Carrero, S., Anderson, C., Dewey, C., Keiluweit, M., Conrad, M., et al. (2022).

875            Sulfur Biogeochemical Cycling and Redox Dynamics in a Shale-Dominated

876            Mountainous Watershed. *Journal of Geophysical Research: Biogeosciences*, *127*(6).

877            https://doi.org/10.1029/2021JG006769

878 Godsey, S. E., Kirchner, J. W., & Clow, D. W. (2009). Concentration-discharge relationships

879            reflect chemostatic characteristics of US catchments. *Hydrological Processes*, *23*(13),

880            1844–1864. https://doi.org/10.1002/hyp.7315

881 Gomez-Velez, J. D., Harvey, J. W., Cardenas, M. B., & Kiel, B. (2015). Denitrification in the

882            Mississippi River network controlled by flow through river bedforms. *Nature*

883            *Geoscience*, *8*(12), 941–945. https://doi.org/10.1038/ngeo2567

884 Goodale, C. L. (2017). Multiyear fate of a [15] N tracer in a mixed deciduous forest: retention,

885            redistribution, and differences by mycorrhizal association. *Global Change Biology*, *23*(2),

886            867–880. https://doi.org/10.1111/gcb.13483

887 Gosz, J. R. (1981). Nitrogen cycling in coniferous forests. *Ecological Bulletins*, *30*, 405–426.

888 Granger, J., & Wankel, S. D. (2016). Isotopic overprinting of nitrification on denitrification as a

889            ubiquitous and unifying feature of environmental nitrogen cycling. *Proceedings of the*

890        *National Academy of Sciences*, *113*(42), E6391–E6400.

891        https://doi.org/10.1073/pnas.1601383113

892    Gurmesa, G. A., Wang, A., Li, S., Peng, S., de Vries, W., Gundersen, P., et al. (2022). Retention

893        of deposited ammonium and nitrate and its impact on the global forest carbon sink.

894        *Nature Communications*, *13*(1), 880. https://doi.org/10.1038/s41467-022-28345-1

895    Hobbie, E. A., & Högberg, P. (2012). Nitrogen isotopes link mycorrhizal fungi and plants to

896        nitrogen dynamics. *New Phytologist*, *196*(2), 367–382. https://doi.org/10.1111/j.1469-

897        8137.2012.04300.x

898    Holloway, J M, Dahlgren, R. A., Hansen, B., & Casey, W. H. (1998). Contribution of bedrock

899        nitrogen to high nitrate concentrations in stream water. *Nature*, *395*, 4.

900    Holloway, JoAnn M., & Dahlgren, R. A. (2002). Nitrogen in rock: Occurrences and

901        biogeochemical implications: BIOGEOCHEMICAL IMPLICATIONS OF N IN ROCK.

902        *Global Biogeochemical Cycles*, *16*(4), 65-1-65–17.

903        https://doi.org/10.1029/2002GB001862

904    Houlton, B. Z., Morford, S. L., & Dahlgren, R. A. (2018). Convergent evidence for widespread

905        rock nitrogen sources in Earth's surface environment. *Science*, *360*(6384), 58–62.

906        https://doi.org/10.1126/science.aan4399

907    Hubbard, S. S., Williams, K. H., Agarwal, D., Banfield, J., Beller, H., Bouskill, N., et al. (2018).

908        The East River, Colorado, Watershed: A Mountainous Community Testbed for

909        Improving Predictive Understanding of Multiscale Hydrological–Biogeochemical

910        Dynamics. *Vadose Zone Journal*, *17*(1), 1–25. https://doi.org/10.2136/vzj2018.03.0061

911    Jia, M., Winkler, M. K. H., & Volcke, E. I. P. (2020). Elucidating the Competition between

912        Heterotrophic Denitrification and DNRA Using the Resource-Ratio Theory.

913   *Environmental Science and Technology*, *54*(21), 13953–62.

914   https://doi.org/10.1021/acs.est.0c01776

915 Johnson, H. M., & Stets, E. G. (2020). Nitrate in Streams During Winter Low-Flow Conditions

916   as an Indicator of Legacy Nitrate. *Water Resources Research*, *56*(11).

917   https://doi.org/10.1029/2019WR026996

918 Killham, K. (1990). Nitrification in coniferous forest soils. *Plant and Soil*, *128*(1), 31–44.

919   https://doi.org/10.1007/BF00009394

920 Knapp, J. L. A., von Freyberg, J., Studer, B., Kiewiet, L., & Kirchner, J. W. (2020).

921   Concentration–discharge relationships vary among hydrological events, reflecting

922   differences in event characteristics. *Hydrology and Earth System Sciences*, *24*(5), 2561–

923   2576. https://doi.org/10.5194/hess-24-2561-2020

924 Knapp, J. L. A., Li, L., & Musolff, A. (2022). Hydrologic connectivity and source heterogeneity

925   control concentration–discharge relationships. *Hydrological Processes*, *36*(9).

926   https://doi.org/10.1002/hyp.14683

927 Kou, D., Yang, G., Li, F., Feng, X., Zhang, D., Mao, C., et al. (2020). Progressive nitrogen

928   limitation across the Tibetan alpine permafrost region. *Nature Communications*, *11*(1),

929   3331. https://doi.org/10.1038/s41467-020-17169-6

930 Kronzucker, H. J., Siddiqi, M. Y., & Glass, A. D. M. (1997). Conifer root discrimination against

931   soil nitrate and the ecology of forest succession. *Nature*, *385*(6611), 59–61.

932   https://doi.org/10.1038/385059a0

933 Lajtha, K. (2020). Nutrient retention and loss during ecosystem succession: revisiting a classic

934   model. *Ecology*, *101*(1). https://doi.org/10.1002/ecy.2896

935 Lansdown, K., Heppell, C. M., Trimmer, M., Binley, A., Heathwaite, A. L., Byrne, P., & Zhang,

936       H. (2015). The interplay between transport and reaction rates as controls on nitrate

937       attenuation in permeable, streambed sediments: Nitrate removal in permeable sediments.

938       *Journal of Geophysical Research: Biogeosciences*, *120*(6), 1093–1109.

939       https://doi.org/10.1002/2014JG002874

940    Leinweber, P., Kruse, J., Baum, C., Arcand, M., Knight, J. D., Farrell, R., et al. (2013).

941       Advances in Understanding Organic Nitrogen Chemistry in Soils Using State-of-the-art

942       Analytical Techniques. In *Advances in Agronomy* (Vol. 119, pp. 83–151). Elsevier.

943       https://doi.org/10.1016/B978-0-12-407247-3.00002-0

944    Leonard, L. T., Mikkelson, K., Hao, Z., Brodie, E. L., Williams, K. H., & Sharp, J. O. (2020). A

945       comparison of lodgepole and spruce needle chemistry impacts on terrestrial

946       biogeochemical processes during isolated decomposition. *PeerJ*, *8*, e9538.

947       https://doi.org/10.7717/peerj.9538

948    Li, D., Wrzesien, M. L., Durand, M., Adam, J., & Lettenmaier, D. P. (2017). How much runoff

949       originates as snow in the western United States, and how will that change in the future?

950       *Geophysical Research Letters*, *44*(12), 6163–6172.

951       https://doi.org/10.1002/2017GL073551

952    Li, L., Sullivan, P. L., Benettin, P., Cirpka, O. A., Bishop, K., Brantley, S. L., et al. (2021).

953       Toward catchment hydro-biogeochemical theories. *WIREs Water*, *8*(1).

954       https://doi.org/10.1002/wat2.1495

955    Li, Y., Schichtel, B. A., Walker, J. T., Schwede, D. B., Chen, X., Lehmann, C. M. B., et al.

956       (2016). Increasing importance of deposition of reduced nitrogen in the United States.

957       *Proceedings of the National Academy of Sciences*, *113*(21), 5874–5879.

958       https://doi.org/10.1073/pnas.1525736113

959 Maavara, T., Siirila-Woodburn, E. R., Maina, F., Maxwell, R. M., Sample, J. E., Chadwick, K.

960     D., et al. (2021). Modeling geogenic and atmospheric nitrogen through the East River

961     Watershed, Colorado Rocky Mountains. *PLOS ONE*, *16*(3), e0247907.

962     https://doi.org/10.1371/journal.pone.0247907

963 Manning, A. H., Verplanck, P. L., Mast, M. L., & Wanty, R. B. (2008). Hydrogeochemical

964     investigation of the Standard Mine vicinity, upper Elk Creek Basin, Colorado (Scientific

965     Investigations Report). USGS.

966 Mason, R. E., Craine, J. M., Lany, N. K., Jonard, M., Ollinger, S. V., Groffman, P. M., et al.

967     (2022). Evidence, causes, and consequences of declining nitrogen availability in

968     terrestrial ecosystems. *Science*, *376*(6590), eabh3767.

969     https://doi.org/10.1126/science.abh3767

970 McDonnell, J. J., Sivapalan, M., Vaché, K., Dunn, S., Grant, G., Haggerty, R., et al. (2007).

971     Moving beyond heterogeneity and process complexity: A new vision for watershed

972     hydrology: Opinion. *Water Resources Research*, *43*(7).

973     https://doi.org/10.1029/2006WR005467

974 Michalski, G., Bhattacharya, S. K., & Mase, D. F. (2012). Oxygen Isotope Dynamics of

975     Atmospheric Nitrate and Its Precursor Molecules. In M. Baskaran (Ed.), *Handbook of*

976     *Environmental Isotope Geochemistry* (pp. 613–635). Berlin, Heidelberg: Springer Berlin

977     Heidelberg. https://doi.org/10.1007/978-3-642-10637-8_30

978 Morford, S. L., Houlton, B. Z., & Dahlgren, R. A. (2011). Increased forest ecosystem carbon and

979     nitrogen storage from nitrogen rich bedrock. *Nature*, *477*(7362), 78–81.

980     https://doi.org/10.1038/nature10415

981 Moyes, A. B., Kueppers, L. M., Pett-Ridge, J., Carper, D. L., Vandehey, N., O'Neil, J., & Frank,

982       A. C. (2016). Evidence for foliar endophytic nitrogen fixation in a widely distributed

983       subalpine conifer. *New Phytologist*, *210*(2), 657–668. https://doi.org/10.1111/nph.13850

984  Musolff, A., Schmidt, C., Selle, B., & Fleckenstein, J. H. (2015). Catchment controls on solute

985       export. *Advances in Water Resources*, *86*, 133–146.

986       https://doi.org/10.1016/j.advwatres.2015.09.026

987  Nardi, P., Laanbroek, H. J., Nicol, G. W., Renella, G., Cardinale, M., Pietramellara, G., et al.

988       (2020). Biological nitrification inhibition in the rhizosphere: determining interactions and

989       impact on microbially mediated processes and potential applications. *FEMS*

990       *Microbiology Reviews*, *44*(6), 874–908. https://doi.org/10.1093/femsre/fuaa037

991  Newcomer, M. E., Bouskill, N. J., Wainwright, H., Maavara, T., Siirila-Woodburn, E. R.,

992       Dwivedi, D., et al. (2021). Hysteresis Patterns of Watershed Nitrogen Retention and Loss

993       Over the Past 50 years in United States Hydrological Basins. *Global Biogeochemical*

994       *Cycles*, 28.

995  Pelletier, J. D., Barron-Gafford, G. A., Gutiérrez-Jurado, H., Hinckley, E.-L. S., Istanbulluoglu,

996       E., McGuire, L. A., et al. (2018). Which way do you lean? Using slope aspect variations

997       to understand Critical Zone processes and feedbacks: Which way do you lean? *Earth*

998       *Surface Processes and Landforms*, *43*(5), 1133–1154. https://doi.org/10.1002/esp.4306

999  Peterson, B. J. (2001). Control of Nitrogen Export from Watersheds by Headwater Streams.

1000       *Science*, *292*(5514), 86–90. https://doi.org/10.1126/science.1056874

1001  Phillips, R. P., Brzostek, E., & Midgley, M. G. (2013). The mycorrhizal-associated nutrient

1002       economy: a new framework for predicting carbon–nutrient couplings in temperate

1003       forests. *New Phytologist*, *199*(1), 41–51. https://doi.org/10.1111/nph.12221

1004  Pinay, G., Peiffer, S., De Dreuzy, J.-R., Krause, S., Hannah, D. M., Fleckenstein, J. H., et al.

1005       (2015). Upscaling Nitrogen Removal Capacity from Local Hotspots to Low Stream

1006       Orders' Drainage Basins. *Ecosystems*, *18*(6), 1101–1120. https://doi.org/10.1007/s10021-

1007       015-9878-5

1008   Rogers, D. B., Newcomer, M. E., Raberg, J. H., Dwivedi, D., Steefel, C., Bouskill, N., et al.

1009       (2021). Modeling the Impact of Riparian Hollows on River Corridor Nitrogen Exports.

1010       *Frontiers in Water*, *3*, 590314. https://doi.org/10.3389/frwa.2021.590314

1011   Rose, L. A., Elliott, E. M., & Adams, M. B. (2015). Triple Nitrate Isotopes Indicate Differing

1012       Nitrate Source Contributions to Streams Across a Nitrogen Saturation Gradient.

1013       *Ecosystems*, *18*(7), 1209–1223. https://doi.org/10.1007/s10021-015-9891-8

1014   Ruddell, B. L., & Kumar, P. (2009). Ecohydrologic process networks: 2. Analysis and

1015       characterization: Ecohydrologic process networks, 2. *Water Resources Research*, *45*(3).

1016       https://doi.org/10.1029/2008WR007280

1017   Schimel, D. S., Braswell, B. H., & Parton, W. J. (1997). Equilibration of the terrestrial water,

1018       nitrogen, and carbon cycles. *Proceedings of the National Academy of Sciences*, *94*(16),

1019       8280–8283. https://doi.org/10.1073/pnas.94.16.8280

1020   Sebestyen, S. D., Shanley, J. B., Boyer, E. W., Kendall, C., & Doctor, D. H. (2014). Coupled

1021       hydrological and biogeochemical processes controlling variability of nitrogen species in

1022       streamflow during autumn in an upland forest: Stream N dynamics during autumn. *Water*

1023       *Resources Research*, *50*(2), 1569–1591. https://doi.org/10.1002/2013WR013670

1024   Sebestyen, S. D., Ross, D. S., Shanley, J. B., Elliott, E. M., Kendall, C., Campbell, J. L., et al.

1025       (2019). Unprocessed Atmospheric Nitrate in Waters of the Northern Forest Region in the

1026       U.S. and Canada. *Environmental Science & Technology*, *53*(7), 3620–3633.

1027       https://doi.org/10.1021/acs.est.9b01276

1028  Sigman, D. M., Casciotti, K. L., Andreani, M., Barford, C., Galanter, M., & Böhlke, J. K. (2001).

1029      A Bacterial Method for the Nitrogen Isotopic Analysis of Nitrate in Seawater and

1030      Freshwater. *Analytical Chemistry*, *73*(17), 4145–4153. https://doi.org/10.1021/ac010088e

1031  Siirila-Woodburn, E. R., Rhoades, A. M., Hatchett, B. J., Huning, L. S., Szinai, J., Tague, C., et

1032      al. (2021). A low-to-no snow future and its impacts on water resources in the western

1033      United States. *Nature Reviews Earth & Environment*, *2*(11), 800–819.

1034      https://doi.org/10.1038/s43017-021-00219-y

1035  Sorensen, P. O., Beller, H. R., Bill, M., Bouskill, N. J., Hubbard, S. S., Karaoz, U., et al. (2020).

1036      The Snowmelt Niche Differentiates Three Microbial Life Strategies That Influence Soil

1037      Nitrogen Availability During and After Winter. *Frontiers in Microbiology*, *11*, 871.

1038      https://doi.org/10.3389/fmicb.2020.00871

1039  Sprenger, M., Carroll, R. W. H., Dennedy-Frank, J, Siirila-Woodburn, E. R., Newcomer, M. E.,

1040      Brown, W., et al. (2022). Variability of Snow and Rainfall Partitioning Into

1041      Evapotranspiration and Summer Runoff Across Nine Mountainous Catchments.

1042      *Geophysical Research Letters*, *49*(13). https://doi.org/10.1029/2022GL099324

1043  Steffen, W., Richardson, K., Rockström, J., Cornell, S. E., Fetzer, I., Bennett, E. M., et al.

1044      (2015). Planetary boundaries: Guiding human development on a changing planet.

1045      *Science*, *347*(6223), 1259855. https://doi.org/10.1126/science.1259855

1046      Tokunaga, T. K., Tran, A. P., Wan, J., Dong, W., Newman, A. W., Beutler, C. A.,

1047      Brown, W., Henderson, A. N., Williams, K. H. (2022). Quantifying subsurface flow and

1048      solute transport in a snowmelt-recharged hillslope with multiyear water balance. Water

1049      Resources Research, 58, *e2022WR032902. https://doi.org/10.1029/2022WR032902*

1050  Thébault, A., Clément, J.-C., Ibanez, S., Roy, J., Geremia, R. A., Pérez, C. A., et al. (2014).

Nitrogen limitation and microbial diversity at the treeline. *Oikos*, *123*(6), 729–740. https://doi.org/10.1111/j.1600-0706.2013.00860.x

Thompson, S. E., Basu, N. B., Lascurain, J., Aubeneau, A., & Rao, P. S. C. (2011). Relative dominance of hydrologic versus biogeochemical factors on solute export across impact gradients: Hydrology controls solute export. *Water Resources Research*, *47*(10). https://doi.org/10.1029/2010WR009605

Uhlemann, S., Dafflon, B., Wainwright, H. M., Williams, K. H., Minsley, B., Zamudio, K., et al. (2022). Surface parameters and bedrock properties covary across a mountainous watershed: Insights from machine learning and geophysics. *Science Advances*, *8*(12), eabj2479. https://doi.org/10.1126/sciadv.abj2479

Wainwright, H. M., Uhlemann, S., Franklin, M., Falco, N., Bouskill, N. J., Newcomer, M. E., et al. (2022). Watershed zonation through hillslope clustering for tractably quantifying above- and below-ground watershed heterogeneity and functions. *Hydrology and Earth System Sciences*, *26*(2), 429–444. https://doi.org/10.5194/hess-26-429-2022

Walker, J. T., Beachley, G., Amos, H. M., Baron, J. S., Bash, J., Baumgardner, R., et al. (2019). Toward the improvement of total nitrogen deposition budgets in the United States. *Science of The Total Environment*, *691*, 1328–1352. https://doi.org/10.1016/j.scitotenv.2019.07.058

Wan, J., Tokunaga, T. K., Williams, K. H., Dong, W., Brown, W., Henderson, A. N., et al. (2019). Predicting sedimentary bedrock subsurface weathering fronts and weathering rates. *Scientific Reports*, *9*(1), 17198. https://doi.org/10.1038/s41598-019-53205-2

Wan, J., Tokunaga, T. K., Brown, W., Newman, A. W., Dong, W., Bill, M., et al. (2020). Bedrock weathering contributes to subsurface reactive nitrogen and nitrous oxide

1074   emissions. *Nature Geoscience*, (14), 217–224. https://doi.org/10.1038/s41561-021-

1075   00717-0

1076   Ward, E. B., Duguid, M. C., Kuebbing, S. E., Lendemer, J. C., & Bradford, M. A. (2022). The

1077   functional role of ericoid mycorrhizal plants and fungi on carbon and nitrogen dynamics

1078   in forests. *New Phytologist*, 18.

1079   Webb, R. W., Wigmore, O., Jennings, K., Fend, M., & Molotch, N. P. (2020). Hydrologic

1080   connectivity at the hillslope scale through intra-snowpack flow paths during snowmelt.

1081   *Hydrological Processes*, *34*(7), 1616–1629. https://doi.org/10.1002/hyp.13686

1082   Wexler, S. K., Goodale, C. L., McGuire, K. J., Bailey, S. W., & Groffman, P. M. (2014).

1083   Isotopic signals of summer denitrification in a northern hardwood forested catchment.

1084   *Proceedings of the National Academy of Sciences*, *111*(46), 16413–16418.

1085   https://doi.org/10.1073/pnas.1404321111

1086   Winnick, M. J., Carroll, R. W. H., Williams, K. H., Maxwell, R. M., Dong, W., & Maher, K.

1087   (2017). Snowmelt controls on concentration-discharge relationships and the balance of

1088   oxidative and acid-base weathering fluxes in an alpine catchment, East River, Colorado:

1089   Acid-base versus oxidative weathering fluxes. *Water Resources Research*, *53*(3), 2507–

1090   2523. https://doi.org/10.1002/2016WR019724

1091   Woelber, B., Maneta, M. P., Harper, J., Jencso, K. G., Gardner, W. P., Wilcox, A. C., & López-

1092   Moreno, I. (2018). The influence of diurnal snowmelt and transpiration on hillslope

1093   throughflow and stream response. *Hydrology and Earth System Sciences*, *22*(8), 4295–

1094   4310. https://doi.org/10.5194/hess-22-4295-2018

1095   Yuan, K., Zhu, Q., Li, F., Riley, W. J., Torn, M., Chu, H., et al. (2022). Causality guided

1096   machine learning model on wetland CH4 emissions across global wetlands. *Agricultural*

1097      *and Forest Meteorology*, *324*, 109115. https://doi.org/10.1016/j.agrformet.2022.109115

1098    Zhi, W., & Li, L. (2020). The Shallow and Deep Hypothesis: Subsurface Vertical Chemical

1099      Contrasts Shape Nitrate Export Patterns from Different Land Uses. *Environmental*

1100      *Science & Technology*, acs.est.0c01340. https://doi.org/10.1021/acs.est.0c01340

1101    Zhi, W., Li, L., Dong, W., Brown, W., Kaye, J., Steefel, C., & Williams, K. H. (2019). Distinct

1102      Source Water Chemistry Shapes Contrasting Concentration-Discharge Patterns. *Water*

1103      *Resources Research*, 2018WR024257. https://doi.org/10.1029/2018WR024257

1104    Zhi, W., Williams, K. H., Carroll, R. W. H., Brown, W., Dong, W., Kerins, D., & Li, L. (2020).

1105      Significant stream chemistry response to temperature variations in a high-elevation

1106      mountain watershed. *Communications Earth & Environment*, *1*(1), 43.

1107      https://doi.org/10.1038/s43247-020-00039-w

1108    Zhou, X., Wang, A., Hobbie, E. A., Zhu, F., Qu, Y., Dai, L., et al. (2021). Mature conifers

1109      assimilate nitrate as efficiently as ammonium from soils in four forest plantations. *New*

1110      *Phytologist*, *229*(6), 3184–3194. https://doi.org/10.1111/nph.17110

1111    Zhu, Q., Castellano, M. J., & Yang, G. (2018). Coupling soil water processes and the nitrogen

1112      cycle across spatial scales: Potentials, bottlenecks and solutions. *Earth-Science Reviews*,

1113      *187*, 248–258. https://doi.org/10.1016/j.earscirev.2018.10.005

1114    Zogg, G. P., Zak, D. R., Pregitzer, K. S., & Burton, A. J. (2000). Microbial immobilization and

1115      the retention of anthropogenic nitrate in a Northern hardwood forest. *Ecology*, *81*(7),

1116      1858–1866. https://doi.org/10.1890/0012-9658(2000)081[1858:MIATRO]2.0.CO;2

1117